PAPER

Check for updates

DFT study of superhalogen and superalkali doped graphitic carbon nitride and its non-linear optical properties

Asmat Ullah Khan,[a] Rasheed Ahmad Khera, [ID] *[a] Naveed Anjum,[a] Rao Aqil Shehzad,[a] Saleem Iqbal,[b] Khurshid Ayub [ID] *[c] and Javed Iqbal [ID] *[ad]

DFT calculations are carried out to investigate nonlinear optical (NLO) properties of superhalogen (BCl_4) and superalkali (NLi_4) doped graphitic carbon nitride (GCN). It is noted that the geometries of doped GCN are sufficiently stable. The energy gap for GCN is 3.89 and it reduces to 0.53 eV in our designed molecule **G4**. Change in the dipole and transition dipole moment is observed along with small transition energies which are responsible for higher hyperpolarizabilities. Doped GCN has larger first and second hyperpolarizabilities which are basic requirements for NLO response. The second hyperpolarizability of GCN enhances from 1.59×10^4 to 2.53×10^8 au when doping with BCl_4 and NLi_4. TD-DFT calculations show the absorption maxima of doped GCN range from 700 nm to 1350 nm. EDDM analysis provides information on electronic distribution from excited to ground state. All these consequences show doped GCN can be a promising NLO material.

1. Introduction

Nonlinear optics describes the behavior of light in nonlinear materials and media. While all molecules and materials are nonlinear to some extent, in most cases the optical properties of a substance are not significantly affected by light.[1–4] However, for sufficiently intense light (typically from strong lasers), one can observe nonlinear optical phenomena related to the way intense light alters the optical properties of material systems. Mathematically, nonlinear materials have a response that depends on the strength of the applied field in a nonlinear manner. For example, in conventional or linear optics, the dipole moment per unit volume of a substance (the dielectric polarization) depends on the strength of the applied optical field.[5–9]

For the past few decades, nonlinear optical (NLO) materials have earned great attention in the field of photonics because of their vast applications in LASER, LED, optical display, biosensors, scanners and telecommunication and other fields of photonics.[6,10–14] Due to their unique properties of producing new electric and magnetic fields, a large number of NLO materials are produced.[15,16] Two major classes of NLO materials are organic and inorganic NLO materials. Organic NLO materials are more

valuable because of their better electronic properties, structural diversity and large NLO coefficient. Inorganic NLO materials also have advantages of their large size, strengths and stability.[17]

Several new inorganic and organic materials are synthesized with improved properties. Inorganic phosphides and nitrides, for example, BP, AlP, BN, AlN and GCN[18] can be largely applied in semiconductors, and other electronic and NLO applications.[19–22] There are more efficient materials for many applications and they can be easily synthesized with low cost.[23]

Nonlinear optical (NLO) properties of molecules and polymers[24–27] are a subject of high importance in organic chemistry and materials sciences. The theoretical prediction of NLO properties based on quantum chemical calculations is challenging and the development of new, along with improvement of existing, methodology remains a substantial demand for computational chemistry.[28–31] The difficulties that occur in such calculations are related to the fact that the NLO properties render themselves inelastic quantities because they are high-order derivatives of the energy.[32–34] Theoretical investigations have shown that the first hyperpolarizability of inorganic and organic molecules is enhanced by a good approach that is doping of superalkali and superhalogen. Superhalogen comprises electronegative atoms (Cl, F and O) which surrounded the central metal atom. By increasing the electronegative atoms, the added electron is delocalized over the metal atom which increases its electron affinity (EA). The electron affinity of superhalogen goes beyond the electron affinity of the halogen atom. The doping of superalkali leads to the generation of alkalide or electride which increases the value of the first hyperpolarizability. Superalkalis have a lower ionization prospective than alkali metals. The nonlinear response of materials

[a]Department of Chemistry, University of Agriculture, Faisalabad-38000, Pakistan. E-mail: Javed.Iqbal@uaf.edu.pk

[b]Department of Chemical Engineering, Wah Engineering College, University of Wah, Wah Cantt, 47040, Pakistan

[c]Department of Chemistry, COMSATS University, Abbottabad Campus, Islamabad, KPK 22060, Pakistan

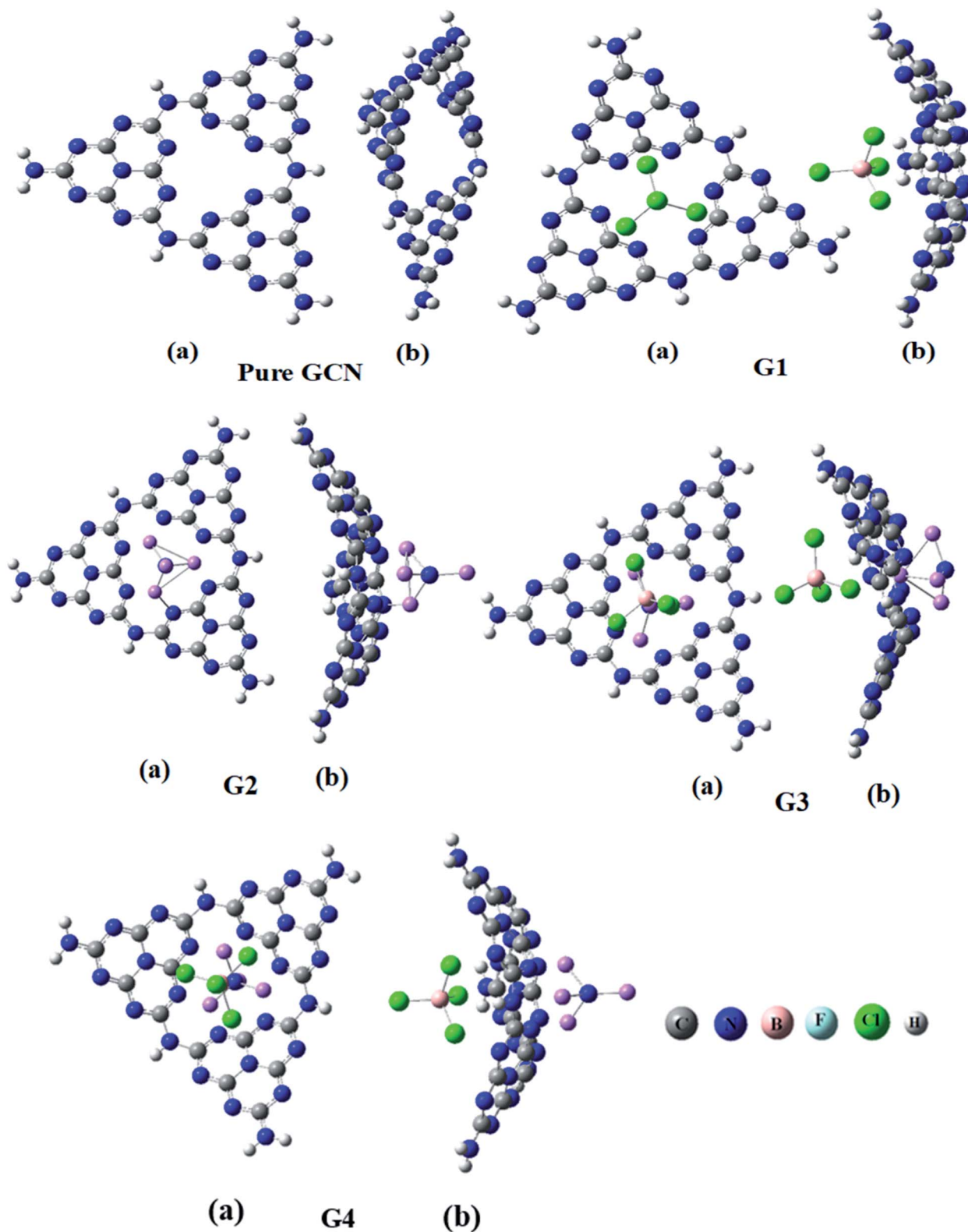[d]Punjab Bio-energy Institute, University of Agriculture, Faisalabad-38000, Pakistan

Fig. 1 Optimized geometries of pure GCN and **G1–G4**.

leads to many optical phenomena including changes in the optical properties of the material, generation of new light frequencies, and changes in the phase or the amplitude of the emergent light.[35,36]

Liebig reported carbon nitride in 1834 for the first time.[37] The GCN has been applied successfully in solar cells, gas and humidity sensors, for the storage of H_2 and CO_2 (ref. 38 and 39) and many others because GCN is thermally stable with a unique

Table 1 The band gap of α-C_3N_4, β-C_3N_4, cubic-C_3N_4, pseudocubic C_3N_4, g-h-triazine, g-o-triazine and g-h-heptazine.[50]

Molecule	Band gap eV
α-C_3N_4	5.49
β-C_3N_4	4.85
Cubic-C_3N_4	4.3
Pseudocubic C_3N_4	4.13
g-h-triazine	2.97
g-o-triazine	0.97
g-h-heptazine	2.88

electronic framework. In recent years, the NLO response of carbon nanostructures that were sp^2 hybridized was largely studied.[40,41] In this study, the graphitic carbon nitride cluster ($C_{18}N_{27}H_8$) was doped with superhalogen (BCl_4) and superalkali (NLi_4). Doping of superhalogen (BCl_4) and superalkali (NLi_4) is an effective way to enhance the NLO response of GCN. Four different complexes of superhalogen (BCl_4) and superalkali (NLi_4) doped GCN were investigated through density functional theory (DFT).[42–44] This study focused on the NLO response, electronic and molecular structure.

2. Computational details

With Gaussian 09 program[45] all the calculations were performed. Structures of the molecules were drawn through GaussView 5.0.[46,47] 6B3LYP method of DFT was used for the geometry optimization and all other calculations with 6-31G (d,p) basis set. 6B3LYP method is quite reliable for geometry optimization and electronic properties of carbon nitride
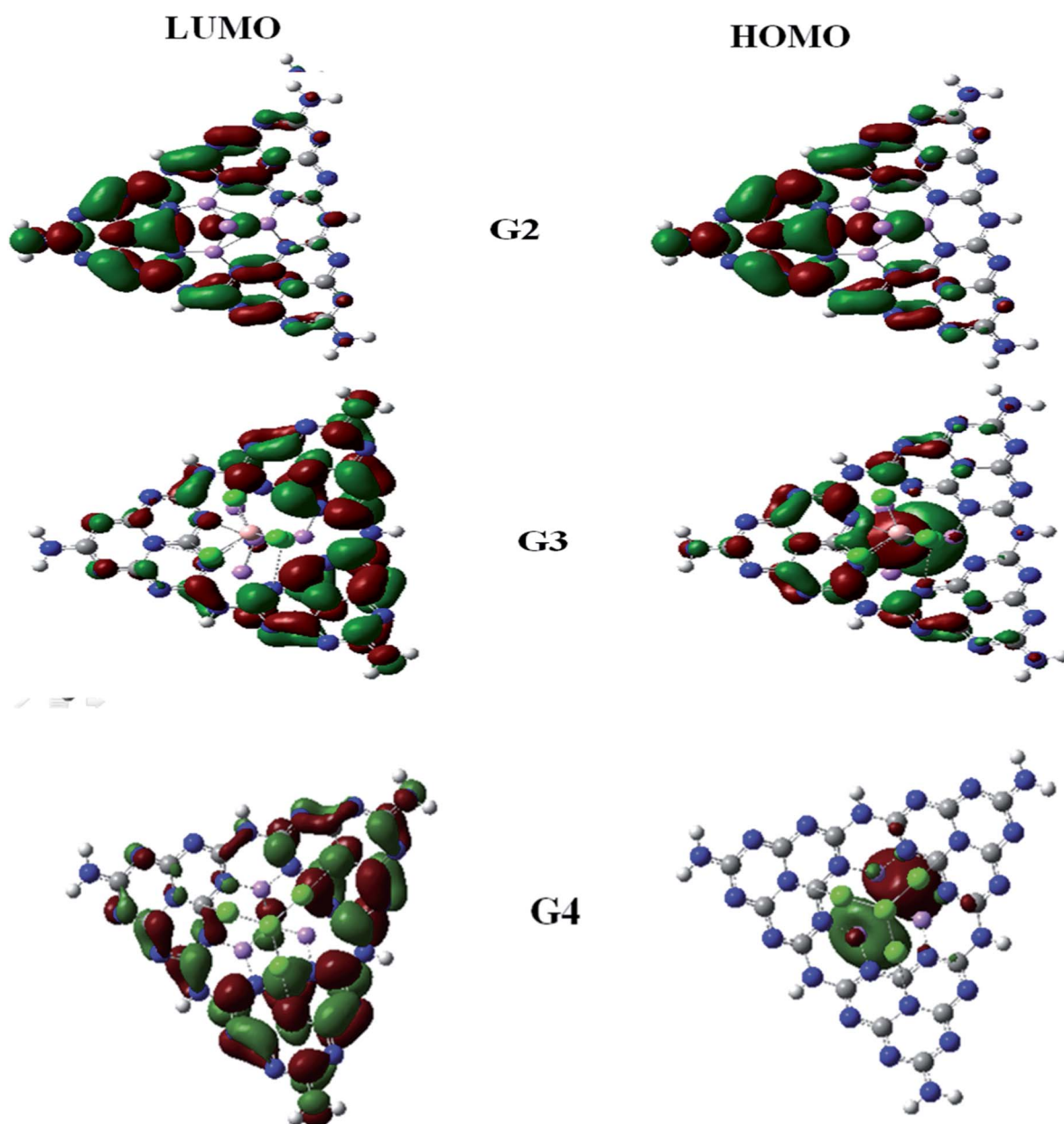

Fig. 2   HOMO LUMO for pure GCN and **G1–G4**.

Table 2   Energies of HOMO, LUMO for pure GCN and **G1–G4**

Molecule	HOMO (eV)	LUMO (eV)
Pure GCN	−6.1	−2.22
G1	−6.37	−2.65
G2	−3.14	−2.38
G3	−3.57	−2.78
G4	−3.59	−2.61

Table 3   Energy gaps and vertical ionization energies for pure GCN and **G1–G4**

Molecule		E_g (eV)	VIE (eV)
Pure GCN		3.89	6.1
G1		3.72	6.37
G2	0.75	3.14	
G3	0.79	3.57	
G4	0.98	3.59	

nanosheets.[48] Energies of HOMO, LUMO and HOMO–LUMO band gap were also computed. The DOS analysis was calculated and plotted by using PyMOlyze software.[49]

The HOMO–LUMO band gap was calculated by eqn (1)

$$E_{H-L} = E_L - E_H \qquad (1)$$

Here E_L, E_H and E_{H-L} are the energies of LUMO, HOMO and HOMO–LUMO.

Vertical Ionization Energies (VIE) were also computed by using the B3LYP method by using eqn (2).

$$VIE = E(X^+) - E(X) \qquad (2)$$

Here $E(X^+)$ and $E(X)$ are the energies of the cation and neutral doped complexes.

B3LYP method was also used to compute values of dipole moment, transition dipole moment, energy of excitation (ΔE), α_{iso} and α_{aniso}, first and second hyperpolarizabilities (β_{static}, γ_{static}) and oscillator strength (f_o). Energy Difference Diagram Map (EDDM) analysis was also performed using the B3LYP method. TD-DFT method was used for UV/Vis absorption analysis and 20 excited states were studied. With the help of Origin software, the UV/Vis spectra were plotted.

3. Results and discussions

3.1. Geometric parameters

Four different superhalogen (BCL_4) and superalkali (NLi_4) doped complexes were optimized at the B3LYP/6-31G (d,p), level of theory. Pure GCN and doped GCN (**G1–G4**) were successfully optimized at B3LYP/6-31G(d,p). **G1** and **G2** contained superhalogen and superalkali on the GCN surface. **G3** & **G4** contained both superhalogen and superalkali on the same molecule but opposite sides. **G3** and **G4** contained superhalogen on bowl-inside and superalkali on bowl-outside. **G3** and **G4** both contain superhalogen on the bowl-in side of GCN, but they differ in the orientation of superalkali on the other side of GCN. In **G3**, the nitrogen atoms of superalkali are pointing away from the GCN surface whereas, in **G4**, a lithium atom is present at the end. It was noted that all the doped complexes were satisfactory stable. Carbon–nitrogen bond lengths (C=N) were computed for pure and all doped complexes. It was examined that, for pure GCN, carbon–nitrogen bonds (C=N) were 1.32 Å. C=N bond lengths were increased from 1.32 Å for pure GCN to 1.34, 1.35, 1.38 Å for **G1**, **G3** & **G4**, respectively. On the other hand, the C=N bond length in **G2** was decreased to 1.30 Å. Front and side
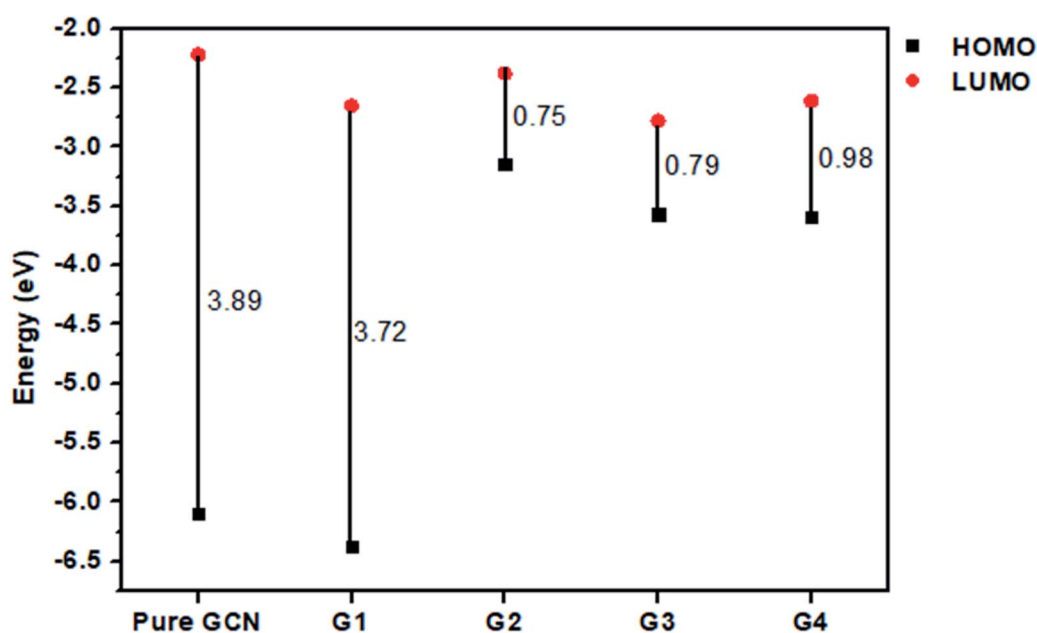

Fig. 3   Energy band gaps for pure GCN and **G1–G4** complexes.

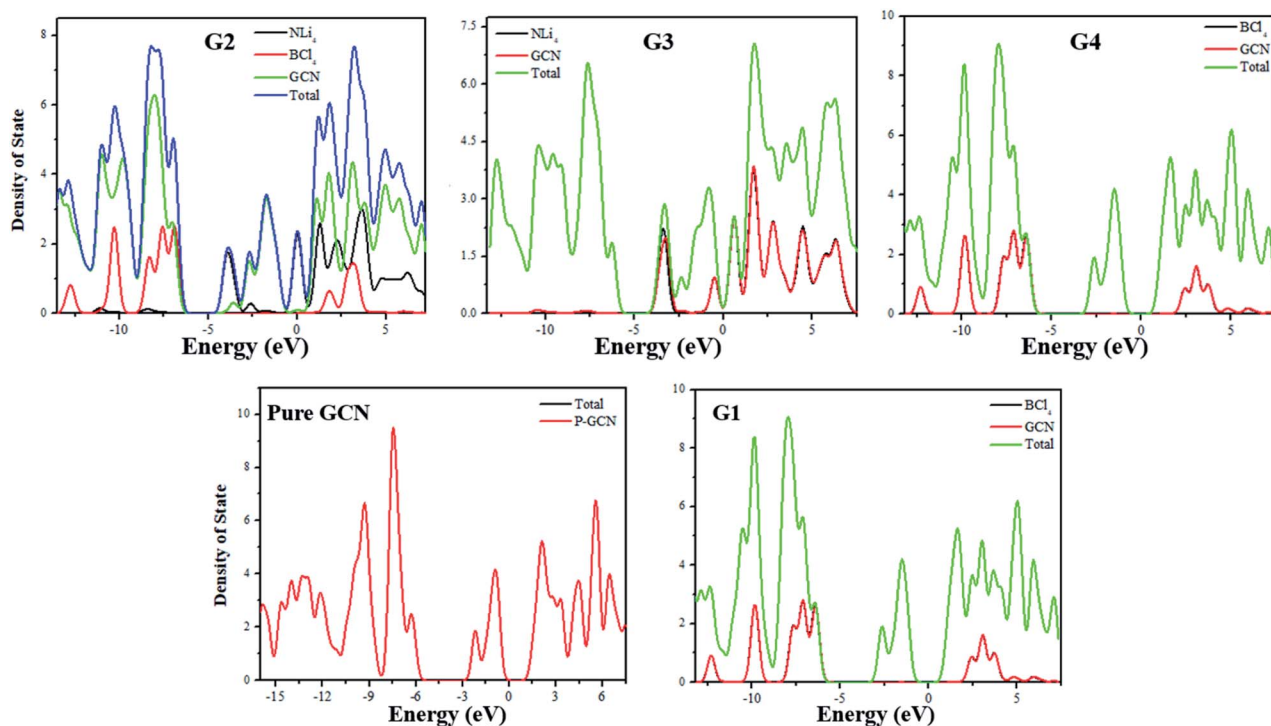

Fig. 4   DOS plots for pure GCN and **G1–G4** complexes.

views (a and b respectively) of optimized geometries for pure GCN and doped **G1–G4** complexes are shown in Fig. 1.

Reported DFT calculations for band gap for different forms of C_3N_4 are listed in Table 1. The band gap of α-C_3N_4, β-C_3N_4, cubic-C_3N_4, pseudocubic C_3N_4, g-h-triazine, g-o-triazine and g-h-heptazine is 5.49 eV, 4.85 eV, 4.30 eV, 4.13 eV, 2.97 eV, 0.93 eV and 2.88 eV, respectively.[50] Two major types of g-C_3N_4 are s-triazine and tri-s-triazine that are linked with tertiary amine groups. Tri-s-triazine is more stable and showed excellent structural, nonlinear optical and physiological properties. The band gap for our proposed form of g-C_3N_4 (tri-s-triazine) is 3.89 eV. Literature study show that our selected model of g-C_3N_4 is a highly stable isomeric form among the other reported forms of g-C_3N_4.[50]

For understanding the electrical and optical properties of the pure GCN and all the designed **G1–G4** molecules, energies of HOMO, LUMO and their H–L gaps were calculated. HOMO is electron-rich and represents the donating ability of the molecule. Whereas LUMO illustrates the electron-withdrawing ability. The FMOs (Frontier Molecular Orbitals) of pure GCN and designed molecules (**G1–G4**) using B3LYP/6-31G (d,p) are shown in Fig. 2. The E_{HOMO} of pure GCN and **G1, G2, G3** and **G4** are −6.10, −6.37, −3.14, −3.57 and −3.59 eV, respectively, while the E_{LUMO} of pure GCN and **G1, G2, G3** and **G4** are −2.22, −2.65, −2.38, −2.78 and −2.61 eV respectively given in Table 2. Doping of BCl_4 and NLi_4 on GCN reduces its energy as new energy levels are generated among these molecules that narrow the energy difference. The energy gap (E_g) for pure GCN and **G1, G2, G3** and **G4** are 3.89, 3.72, 0.75, 0.79 and 0.98 eV, respectively. This reduction of the energy gap enhances its electronic conduction and makes it easy for electrons to excite from HOMO to LUMO.

The decreasing order of E_g is pure GCN > **G1** > **G4** > **G3** > **G2**. HOMO and LUMO energy gap of **G1–G4** are low as compared with pure GCN. The **G1** molecule has the highest energy gap of 3.72 eV (Fig. 3).

Vertical ionization energies for all doped complexes were also computed and their values are 6.10, 6.37, 3.14, 3.57 and 3.59 eV of pure GCN and **G1, G2, G3** and **G4**, respectively. The decreasing order for VIE of all pure and doped complexes is pure GCN > **G1** > **G4** > **G3** > **G2**. All the values are given in Table 3.

For the understanding of the HOMO–LUMO gap reduction, the density of states (DOS) analysis was performed at the same level of theory. DOS plot for pure GCN showed that there is a large gap between HOMO and LUMO. In the analysis of the DOS plot of **G1–G4**, a reduction of the energy gap was observed for all complexes. In **G1**, superhalogen donates excess electrons to GCN and because of these electrons, new energy levels are formed which are responsible for the reduction of the energy gap. Superhalogen, without such excess electrons, does not cause any decrease in the H–L gap. All these new energy levels formed between the original HOMOs and LUMOs of pure GCN result in the reduction of the energy gap. PDOS represents the partial DOS analysis of individual superalkali, superhalogen and GCN fragments whereas, TDOS represents the total DOS analysis of doped molecule. In the DOS plots, TDOS for pure GCN (Redlined) in the range of −16 to −5 eV represents occupied states whereas −2 to 9 eV represent virtual states. In the case of **G1**, PDOS of pure GCN and TDOS of doped GCN (indicated by red and green lines) ranging from −16 to −5 eV represent HOMO and from −2 to 9 eV represent LUMO but the doped GCN exhibit sharp green peaks in its TDOS
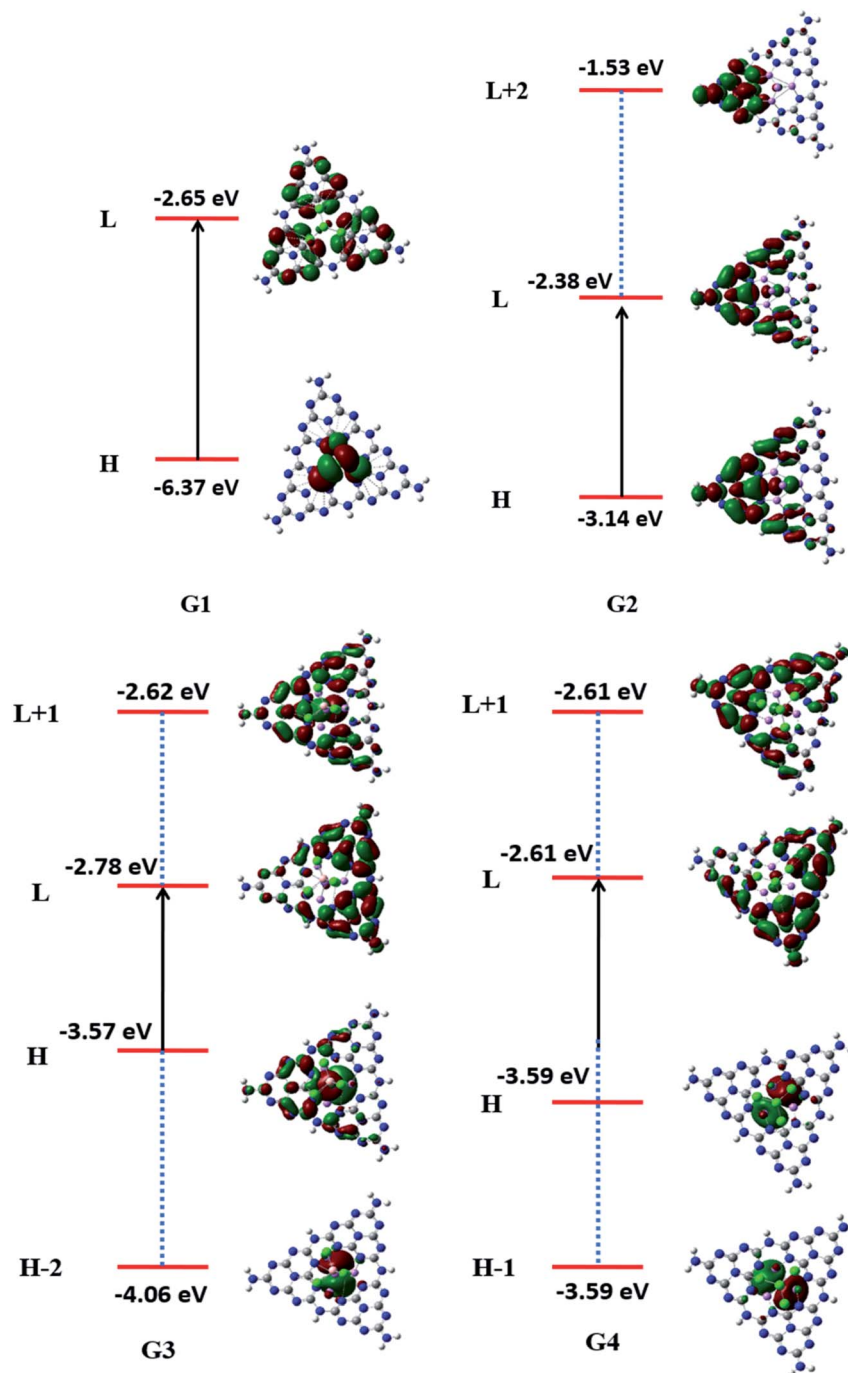
Fig. 5   Transition diagrams pure GCN and G1–G4 complexes.

representation which is ascribed for the dominant effect of doping in reducing energy gap. In the DOS plot of **G2**, PDOS of individual superalkali (NLi_4), superhalogen (BCl_4) and GCN (indicated by black Red and green lines) and TDOS of doped GCN (indicated by the blue line), ranging from −13 to −5 eV represent HOMO and from −4 to 9 eV represent LUMO and LUMO+2. The sharp blue peaks indicate the greater contribution of electron density from doped GCN as well as the higher HOMO and lower LUMO energy levels of **G2** become the cause for reduction of the energy gap. In the DOS plot of **G3**, PDOS of
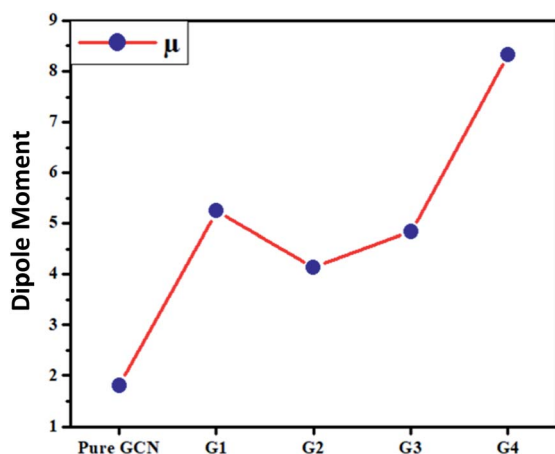
Table 4   Dipole moment transition dipole moment for pure GCN and G1–G4

Molecule	μ (D)	$\Delta\mu$ (D)
Pure GCN	1.81	
G1	5.24	0.0192
G2	4.14	0.1235
G3	4.84	0.0237
G4	8.33	0.0052

Table 5 Linear isotropic and anisotropic for pure GCN and **G1–G4**

| Molecule	α_{iso} (au)	α_{aniso} (au)
Pure GCN	437.54	438.89
G1	932.39	659.13
G2	745.64	512.73
G3	723.89	453.29
G4	656.01	198.63

Fig. 6 Dipole moment (μ) for pure GCN and **G1–G4**.

superalkali (NLi_4) and pure GCN and TDOS of doped GCN (indicated by black, red and green lines respectively) ranging from -14 to -4 eV represent HOMO and HOMO-2 and from -5 to 9 eV represent LUMO and LUMO+1. The flat red peak of pure GCN in the HOMO region shows its little electronic contribution but the sharp green peaks of doped GCN plausibly explain the high

electronic contribution due to the strong effect of dopant in reducing the energy gap. Similar is the case with **G4**. DOS plots for pure GCN and **G1–G4** are shown in Fig. 4.

To understand the nature of excitation, orbital transitions analysis was performed for pure and doped complexes. For pure GCN and **G1**, the transition took place from HOMO to LUMO, whereas in **G2**, the transition took place from HOMO to LUMO+2. For **G3** transition took place from HOMO-2 to LUMO+1 whereas it is from HOMO-1 to LUMO+1 in **G4**. These new energy levels which were formed between the original HOMO and LUMO are the evidence of reduction of the energy gap. All these transitions are graphically represented in Fig. 5.

3.2. Non-linear optical properties

The dipole moments for pure GCN and **G1–G4** were computed and it was noted that the dipole moment was changed on doping superhalogen and superalkali on GCN. For pure GCN, it is 1.81 D whereas dipole moments are 5.24, 4.14, 4.84 and 8.33 D for **G1**, **G2**, **G3** and **G4**, respectively. The increasing order of dipole moment is pure GCN < **G2** < **G3** < **G1** < **G4**. Pure GCN has a low dipole moment due to the symmetry and this symmetry is broken when a dopant is introduced on GCN. Among the doped structures, **G1** and **G2** are singly doped either containing superalkali or a super halogen whereas **G3** and **G4** contain both superakali and superhalogen on the opposite faces of the GCN sheet. In **G3** and **G4**, the superalkali serves as a source of electrons whereas superhalogen is the acceptor moiety. A deep analysis reveals that the dipole moments are higher for systems containing superhalogen and the dipole moment vector in these complexes starts from the halogen of BCl_4 and ends up towards the GCN surface. **G3** and **G4** both contain superhalogen on the bowl-in side of GCN, but they differ in
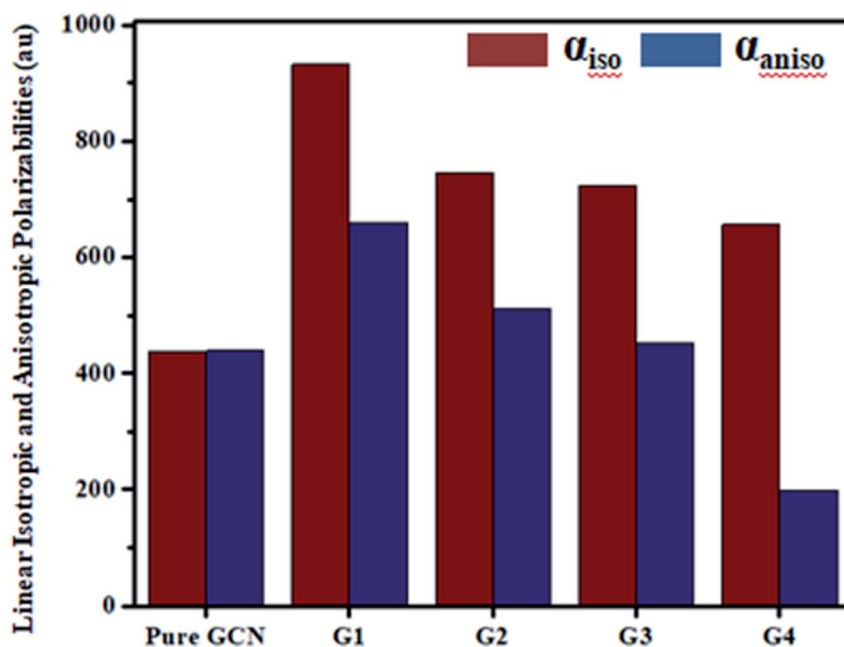
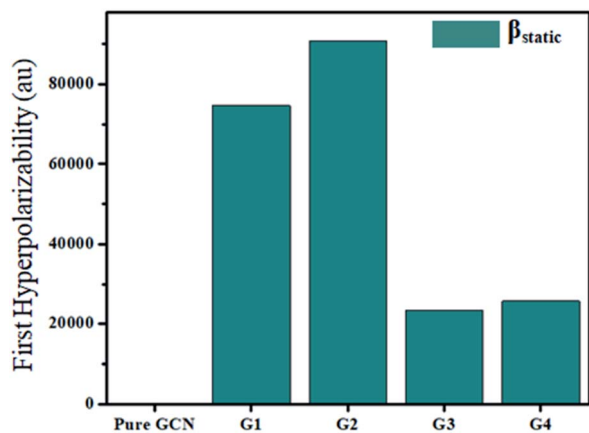**Fig. 7** First hyperpolarizability (β_{static}) for pure GCN and **G1–G4**.

Fig. 8 Linear isotropic (α_{iso}) and anisotropic (α_{aniso}) polarizabilities for pure and **G1–G4**.

the orientation of superalkali on the other side of GCN. In **G3**, the nitrogen atoms of superalkali are pointing away from the GCN surface whereas, in **G4**, a lithium atom is present at the end. The presence of a lithium atom at the end in **G4** creates a positive pole whereas a halogen of BCl_4 (on the other end) creates a negative pole. The presence of clear positive and negative poles with a large distance between them leads to a larger dipole moment of **G4** over **G3**. Moreover, the dipole moment vector of **G4** is not on the axis connecting the superalkali with superhalogen rather it is tilted on the side which leads to a lower dipole moment.

The transition dipole moment for pure GCN and **G1–G4** was also computed and it was noted that the transition dipole moments were changed on doping superhalogen and superalkali on GCN. For **G1–G4**, these are 0.0192, 0.1235, 0.0237 and 0.0052 D respectively. The increasing order of transition dipole moment is **G4** < **G1** < **G3** < **G2**. The values of dipole moment transition dipole moment for pure GCN and **G1–G4** are listed in Table 4.

For all complexes linear isotropic and anisotropic polarizabilities (α_{iso} and α_{aniso}) were computed. For pure GCN α_{iso} is 437.54 au and it increased on doping to 932.39, 745.64, 723.89
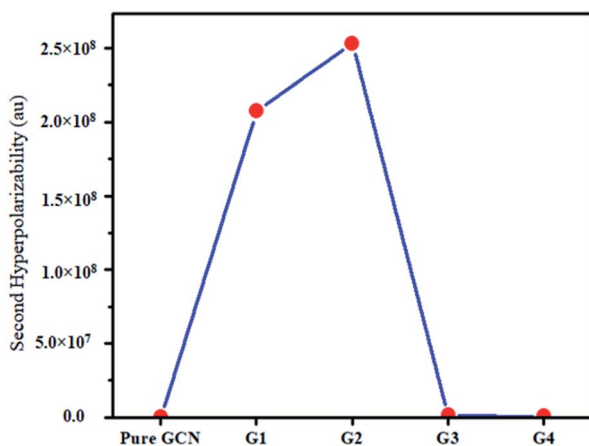

Fig. 9 Second hyperpolarizability for pure GCN and **G1–G4**.

Table 6 First and second hyperpolarizabilities ($\beta_{static}, \gamma_{static}$) for all complexes

Molecule	β_{static} (au)	γ_{static} (au)
Pure GCN	95.37	1.59×10^4
G1	74 703	2.07×10^8
G2	90 733	2.53×10^8
G3	23 325	1.14×10^6
G4	25 738	4.43×10^5

and 656.01 for **G1**, **G2**, **G3** and **G4**, respectively, respectively. Values of α_{iso} increase in order pure GCN < **G4** < **G3** < **G2** < **G1**. α_{aniso} of pure GCN is 438.89 au and it changed on doping to 659.13, 512.73, 453.29 and 198.63 au for **G1**, **G2**, **G3** and **G4**, respectively. α_{aniso} increase in the order **G4** < pure GCN < **G3** < **G2** < **G1**. Values for all complexes linear isotropic and anisotropic are listed in Table 5.

For the NLO response, hyperpolarizability is the major property. First and second hyperpolarizabilities (β_{static} and γ_{static}) were also computed. β_{static} for pure GCN is 95.37 au and β_{static} values are 74 703, 90 733, 23 325 and 25 738 au for **G1**, **G2**, **G3** and **G4**, respectively. β_{static} increased in the order: pure GCN < **G3** < **G4** < **G1** < **G2**. γ static for pure GCN is 1.59×10^4 and values for **G1–G4** are 2.07×10^8, 2.53×10^8, 1.14×10^6 and 4.43×10^5 au respectively. Values of γ_{static} increase in order pure GCN < **G4** < **G3** < **G2** < **G1**. Dipole moment (μ in D), α_{iso} and α_{aniso} in au, β_{static} in au and γ_{static} in au are graphically represented in Fig. 6, Fig. 7, Fig. 8 and Fig. 9, respectively. A two-level approximation is a frequently used model that supports the calculation of nonlinearities especially the first hyperpolarizability as follows.[51]

$$\beta_0 = \frac{\Delta\mu \times f_o}{\Delta E^3} \quad (3)$$

where $\Delta\mu, f_o$ and ΔE^3 are the transition dipole moment from the ground to the excited state, highest oscillator strength and transition energy for the crucial excitations, respectively. The small values for ΔE of **G1–G4** show that these complexes have larger hyperpolarizabilities. f_o for pure GCN is zero and it was changed for **G1–G4**. The values of f_o are 0.0001, 0.0006, 0.0054 and 0.0035 for **G1–G4**, respectively. Hyperpolarizabilities for all complexes are given in Table 6.

Excitation energy (ΔE) and oscillator strength (f_o) for **G1–G4** are given in Table 7.

Absorption energies of pure GCN and **G1–G4** are computed through time-dependent DFT (TD-DFT). 20 excited states were studied, and it was noted that pure GCN absorbs at 350 nm.

Table 7 Oscillator strength (f_o) and transition orbital for **G1–G4**

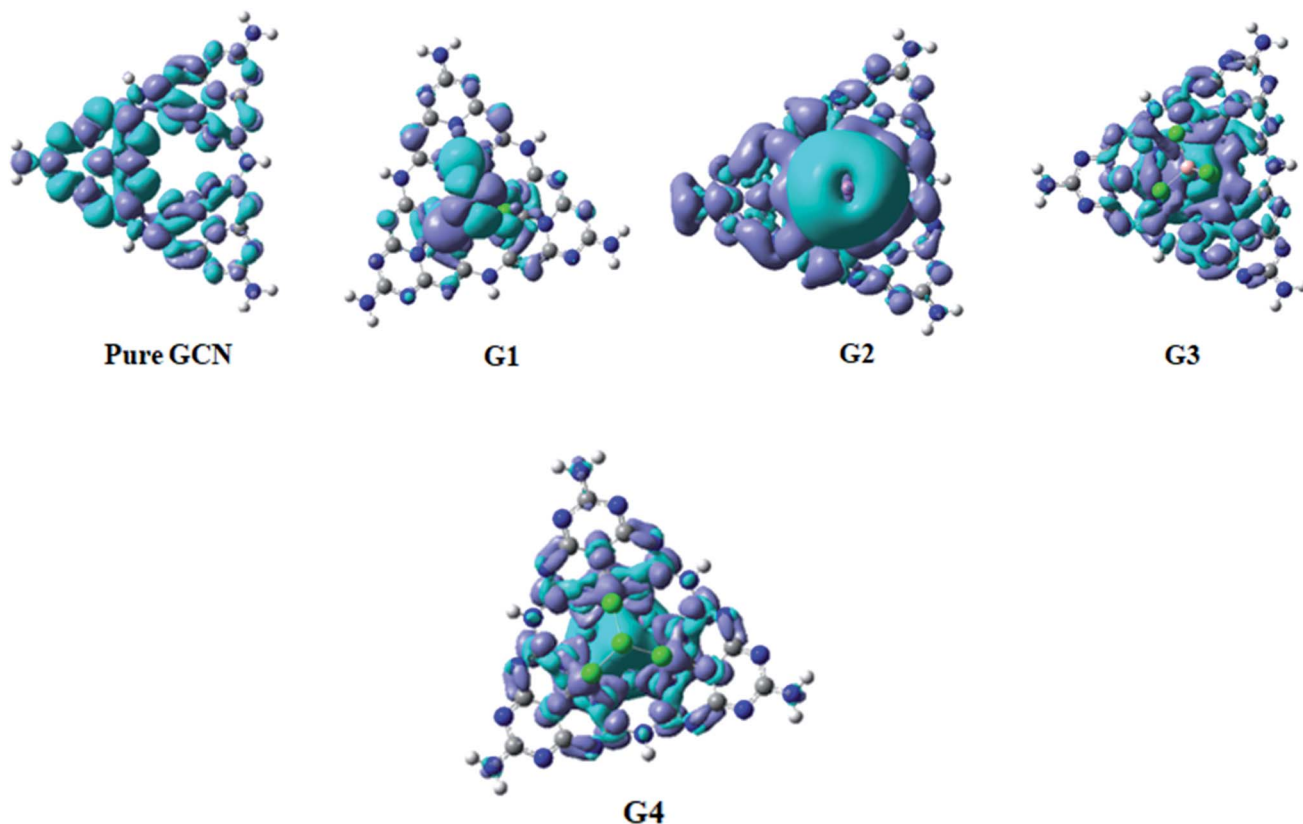| Molecule	f_o	ΔE eV
G1	0.0001	0.0283
G2	0.0006	0.2378
G3	0.0054	0.1068
G4	0.0035	0.422

Fig. 10 UV-vis spectra for pure GCN and **G1–G4**.

Table 8 Absorption (λ_{max}) and transition orbital for **G1–G4**

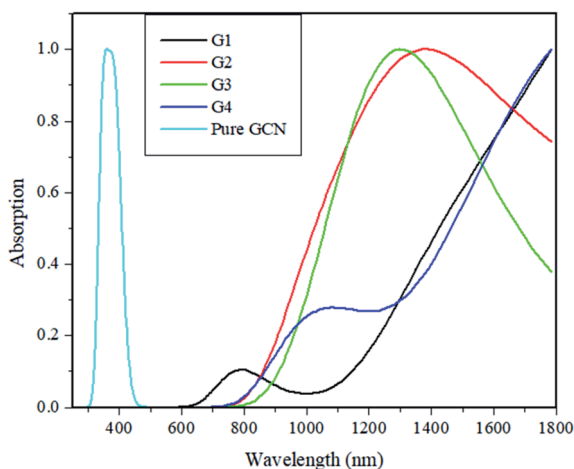| Molecule	λ_{max} (nm)	% C.I transition
G1	780	97% H → L
G2	1350	96% H → L+2
G3	1290	84% H-2 → L+1
G4	1045	50% H-1 → L+1

Fig. 11 EDDM of pure GCN and **G1–G4**.

After doping superhalogen and superalkali absorption maxima are red-shifted. All the doped structures absorb radiations in the visible and IR region. The λ_{max} for **G1, G2, G3** and **G4** are 780, 1350, 1290 and 1045 nm. This shows that these doped complexes have valuable absorption for NLO response. Absorption spectra for pure GCN and **G1–G4** are shown in Fig. 10. Absorption (λ_{max}) and transition orbital for **G1–G4** are listed in Table 8.

3.3. EDDM analysis

Electron Density Difference Map (EDDM) analysis of pure GCN and **G1–G4** complexes was carried out at the B3LYP/6-31G level of theory. For a better understanding of resultant charge density over the molecule, EDDM analysis was carried out. Images of EDDM gave information about the electronic distribution of pure GCN and doped complexes **G1–G4** from excited to ground state transition ($\rho_{excited} - \rho_{ground}$). Two different colors were seen in EDDM images (sea-green and purple color). The reduced density of electrons shown in purple color with a negative value and electron reorganizations with a positive value with sea-green color represents the electronic density growth. EDDM images for pure GCN and doped **G1–G4** are shown in Fig. 11.

4. Conclusions

NLO response of superhalogen (BCL_4) and superalkali (NLi_4) doped graphitic carbon nitride (GCN) was investigated by

density field theory (DFT) methods. It was noted that all the doped complexes (**G1–G4**) were geometrically stable. Reduction of HOMO–LUMO energy gap was noted for all **G1–G4**. For pure GCN, the energy gap is 3.89 eV. **G1** showed the highest energy gap of 3.72 eV among doped clusters. VIEs for all **G1–G4** were changed for all **G1–G4**. The increase in dipole moment was observed for **G1–G4**. It was also observed that the values of ΔE were small which indicates higher values of hyperpolarizabilities. Doping of superhalogen and superalkali on GCN change linear isotropic and anisotropic polarizabilities which are responsible for their NLO response. Moreover, the first and second hyperpolarizability (β_{static} and γ_{static}) were changed. β_{static} for pure GCN was 95.37 au and for **G3** it was increased to 90 733 au. All these changes after doping enhanced the NLO response of GCN. All the doped complexes show absorption in the range of 700 to 1350 nm. All the results propose that superhalogen and superalkali co-doped graphitic carbon nitride (**G1–G4**) can be promising candidates as NLO material.

Conflicts of interest

There are no conflicts to declare.

Acknowledgements

References

1 X. Xue, H. Wang, Y. Han and H. Hou, *Dalton Trans.*, 2018, **47**, 13–22.

2 A. A. A. Aziz, F. M. Elantabli, H. Moustafa and S. M. El-Medani, *J. Mol. Struct.*, 2017, **1141**, 563–576.

3 T. V. Vu, A. Lavrentyev, B. Gabrelian, O. Parasyuk and O. Khyzhun, *Mater. Chem. Phys.*, 2018, **219**, 162–174.

4 Ö. Tamer, D. Avcı and Y. Atalay, *J. Phys. Chem. Solids*, 2016, **99**, 124–133.

5 V. Sivasubramani, V. Mohankumar, M. S. Pandian and P. Ramasamy, *CrystEngComm*, 2017, **19**, 5662–5678.

6 S. Ding, C. Wang, X. Shi, J. Zou, Q. Cheng, J. Zhu, Z. Shi, Z. Cai, C. Chen and Z. Cui, *J. Mater. Chem. C*, 2019, **7**, 4667–4672.

7 T. Verbiest, D. Burland, M. Jurich, V. Lee, R. Miller and W. Volksen, *Science*, 1995, **268**, 1604–1606.

8 N. Dhumane, S. Hussaini, V. Dongre and M. D. Shirsat, *Opt. Mater.*, 2008, **31**, 328–332.

9 P. S. Halasyamani and W. Zhang, *Inorg. Chem.*, 2017, **56**(20), 12077–12085.

10 B. Panunzi, R. Diana, A. Tuzi, A. Carella and U. Caruso, *J. Mol. Struct.*, 2019, **1189**, 21–27.

11 K. Kamatchi, P. Umarani, T. Radhakrishnan and C. R. Raja, *Optik*, 2018, **172**, 674–679.

12 S. Goel, N. Sinha, H. Yadav, A. J. Joseph, A. Hussain and B. Kumar, *Arabian J. Chem.*, 2020, **13**, 146–159.

13 L. Mydlova, S. Taboukhat, A. Ayadi, A. Migalska-Zalas, A. El-Ghayoury, A. Zawadzka, M. Makowska-Janusik and B. Sahraoui, *Opt. Mater.*, 2018, **86**, 304–310.

14 B. Mohan, M. Choudhary, S. Bharti, A. Jana, N. Das, S. Muhammad, A. G. Al-Sehemi and S. Kumar, *J. Mol. Struct.*, 2019, **1190**, 54–67.

15 G. Zou and K. M. Ok, *Chem. Sci.*, 2020, **11**, 5404–5409.

16 S.-P. Guo, Y. Chi and G.-C. Guo, *Coord. Chem. Rev.*, 2017, **335**, 44–57.

17 S. Muhammad, *Mater. Chem. Phys.*, 2018, **220**, 286–292.

18 G. Venkatesh, M. Govindaraju, P. Vennila and C. Kamal, *J. Theor. Comput. Chem.*, 2016, **15**, 1650007.

19 J. Iqbal, R. Ludwig and K. Ayub, *Mater. Res. Bull.*, 2017, **92**, 113–122.

20 K. Ayub, *J. Mater. Chem. C*, 2016, **4**, 10919–10934.

21 J. Iqbal and K. Ayub, *J. Alloys Compd.*, 2016, **687**, 976–983.

22 R. A. Shehzad, J. Iqbal, K. Ayub, F. Nawaz, S. Muhammad, A. R. Ayub and S. Iqbal, *Optik*, 2021, **226**, 165923.

23 P. Vennila, M. Govindaraju, G. Venkatesh and C. Kamal, *J. Mol. Struct.*, 2016, **1111**, 151–156.

24 H. S. Nalwa and S. Miyata, *Nonlinear optics of organic molecules and polymers*, CRC press, 1996.

25 J. Messier, P. Prasad and D. Ulrich, *Nonlinear optical effects in organic polymers*, Springer Science & Business Media, 2012.

26 X. Meng, Y. Song, H. Hou, Y. Fan, G. Li and Y. Zhu, *Inorg. Chem.*, 2003, **42**, 1306–1315.

27 J. A. Delaire and K. Nakatani, *Chem. Rev.*, 2000, **100**, 1817–1846.

28 F. Castet, V. Rodriguez, J.-L. Pozzo, L. Ducasse, A. Plaquet and B. Champagne, *Acc. Chem. Res.*, 2013, **46**, 2656–2665.

29 C. Ye, T. J. Marks, J. Yang and G. Wong, *Macromolecules*, 1987, **20**, 2322–2324.

30 J. Qin, D. Liu, C. Dai, C. Chen, B. Wu, C. Yang and C. Zhan, *Coord. Chem. Rev.*, 1999, **188**, 23–34.

31 D. F. Eaton, *Science*, 1991, **253**, 281–287.

32 P. S. Liyanage, R. M. de Silva and K. N. de Silva, *J. Mol. Struct.: THEOCHEM*, 2003, **639**, 195–201.

33 S. D. Bella, *Chem. Soc. Rev.*, 2001, **30**, 355–366.

34 I. C. de Silva, R. M. de Silva and K. N. De Silva, *J. Mol. Struct.: THEOCHEM*, 2005, **728**, 141–145.

35 N. Leclerc, S. Sanaur, L. Galmiche, F. Mathevet, A.-J. Attias, J.-L. Fave, J. Roussel, P. Hapiot, N. Lemaître and B. Geffroy, *Chem. Mater.*, 2005, **17**, 502–513.

36 S. Muhammad, A. G. Al-Sehemi, A. Irfan, H. Algarni, Y. Qiu, H. Xu, Z. Su and J. Iqbal, *J. Mol. Graphics Modell.*, 2018, **81**, 25–31.

37 F. Goettmann, A. Fischer, M. Antonietti and A. Thomas, *Angew. Chem., Int. Ed.*, 2006, **45**, 4467–4471.

38 C.-t. Chen and G.-z. Liu, *Annu. Rev. Mater. Sci.*, 1986, **16**, 203–243.

39 M. E. Wright and M. S. Sigman, *Macromolecules*, 1992, **25**, 6055–6058.

40 K. Sridharan, P. Sreekanth, T. J. Park and R. Philip, *J. Phys. Chem. C*, 2015, **119**, 16314–16320.

41 A. S. Febena, M. V. A. Raj and J. Madhavan, *Mechanics, Materials Science & Engineering Journal*, 2017, DOI: 10.2412/mmse.48.92.693.

42 A. Omidvar, *Inorg. Chem.*, 2018, **57**, 9335–9347.

43 A. K. Srivastava, A. Kumar and N. Misra, *Chem. Phys. Lett.*, 2017, **682**, 20–25.

44 G.-L. Hou and X.-B. Wang, *Chem. Phys. Lett.*, 2020, **741**, 137094.

45 M. Barbatti, M. Ruckenbauer, F. Plasser, J. Pittner, G. Granucci, M. Persico and H. Lischka, *Wiley Interdiscip. Rev.: Comput. Mol. Sci.*, 2014, **4**, 26–33.

46 X.-D. Kai-Xiong and J. Hong, *Chin. J. Spectrosc. Lab.*, 2012, **1**, 058.

47 I. Obot, D. Macdonald and Z. Gasem, *Corros. Sci.*, 2015, **99**, 1–30.

48 M. Yar, M. A. Hashmi and K. Ayub, *RSC Adv.*, 2020, **10**, 31997–32010.

49 N. M. O'boyle, A. L. Tenderholt and K. M. Langner, *J. Comput. Chem.*, 2008, **29**, 839–845.

50 Y. Xu and S.-P. Gao, *Int. J. Hydrogen Energy*, 2012, **37**, 11072–11080.

51 S. Muhammad, H. Xu, Z. Su, K. Fukuda, R. Kishi, Y. Shigeta and M. Nakano, *Dalton Trans.*, 2013, **42**, 15053–15062.